Advanced Physics Lab II

Lab Report #2

Electron Spin & Nuclear Magnetic Resonance

Group 1
Noah Horne, Luka Burduli

11/03/2025

Dr. Arnulf Materny
Dr. Faezeh Mohaghegh

We hereby declare that we (Luka Burduli and Noah Horne) are the sole authors of this lab report and have not used any sources other than those listed in the bibliography and identified as references throughout the report.

_____ _____

Contents

1 Abstract

The results of this investigation strongly support the existence of the phenomena of wave-particle duality. To analyze the nature of particles acting as waves, electron diffraction was analyzed. In the pursuit of this investigation, the lattice spacings of a hexagonal polycrystalline graphite film coated copper lattice were examined and calculated to be $d_1 = (21.5 \pm 2.19) \cdot 10^{-11}$ [m] and $d_2 = (10.5 \pm 1.15) \cdot 10^{-11}$ [m], respectively. To analyze the phenomena of waves acting as particles, the behavior of X-Ray photons and their Compton scattering across a plastic sample was examined. During this investigation, the two transition energies of the copper sample K_α and K_β were determined to be $1.27 \cdot 10^{-15}$ [J] and $1.41 \cdot 10^{-15}$ [J] respectively for 1st order maxima. Furthermore, the Compton wavelength was calculated to reasonable statistical accuracy with a value of $(2.07 \pm 1.76) \cdot 10^{-12}$ [m]. All results obtained during this investigation adhere to the theoretical predictions to a commensurable degree.

2 Introduction & Theory

This investigation focuses on the in-depth analysis and observation of wave-particle duality through the measurement of electron diffraction patterns and the behaviour of Compton scattered photons. In the context of this specific investigation, electron diffraction is measured through the acceleration of an electron beam by a variable anode voltage passed through a polycrystalline graphite film deposited onto a copper grating. As the electrons travel through the hexagonal lattice of the graphite-coated copper grating, spherical diffraction is mediated by the electron beam. Such diffraction is consequently visualized by a diametrically opposed fluorescent screen, and through the diffraction pattern the hexagonal lattice spacing is calculated. As is known from optical physics, diffraction is a wave-like phenomenon. Making use of this fact, one can determine the wave-like properties of massive subatomic particles such as the electron. By nature of this particle wave duality, an associated wavelength λ must be assigned to each particle, directly dependent on their momentum p.

$$\lambda = \frac{h}{p} \tag{2.1}$$

Equation 2.1 bridges the gap between particles and waves through the assignment of a virtual wavelength λ to any momentum p carrying particle, where h is Planck's constant $\approx 6.626 \cdot 10^{-34} Js$ (Materny & Mohaghegh, 2025). Notice then that due to this quantum scaling factor (Planck's Constant) most particles exhibit very small wavelengths. In the case of a non-relativistic electron, these wavelengths λ can range to be only a few picometers in scale. In the context of this investigation, the diffraction exhibiting electrons will be accelerated through the application of an external anode voltage U_A before passing through the polycrystalline film. Rewriting equation 2.1 to take into account the mass of the electron m_e and acceleratory anode voltage U_A, the de-Broglie wavelength λ of the electron transforms formulaically to:

$$\lambda = \frac{h}{\sqrt{2m_e eU_A}} \tag{2.2}$$

where m_e is the mass of the electron and e is the elementary charge. As the voltages used to accelerate these electrons range between 4kV to 7.5kV the relativistic effects on the mass of the electron are negligible to a degree of 0.5% deviation (Materny & Mohaghegh, 2025). As the velocity of the electrons in this experiment are much smaller than the speeds required to exhibit significant relativistic behavior, the lack of consideration for relativistic effects is an appropriate simplification. To determine the lattice spacing of the polycrystalline graphite film coated copper, the diameter of the constructively interferent diffraction rings are measured, and the corresponding Bragg angle calculated–the angle between the incoming beam and the lattice plane of the crystal θ–then the lattice spacing d can be found similarly (Materny & Mohaghegh, 2025). For angles where constructive interference is observed on the fluorescent screen, the so-called Bragg condition between Bragg angle θ, lattice spacing d and de Broglie wavelength λ must be satisfied, e.g:

$$2d \sin\theta = n \cdot \lambda \quad n = 1, 2, 3, \ldots \tag{2.3}$$

When this equation is satisfied, a corresponding maximum is observed due to the occurrence of constructive interference. Alternatively, this behavior can be classified as strong reflection from the polycrystalline graphite lattice. The Bragg angle θ, although not directly measured during this investigation, remains experimentally relevant as it dictates the behavior of the observed diffraction pattern and is closely related to the desired calculated quantity, the lattice spacing d. Furthermore, it is precisely half as large as the angle to the maxima of the diffraction pattern α, e.g. $2\theta = \alpha$. Specifically, one can apply a small angle approximation to the Bragg condition and some trigonometric rearrangment to express the Bragg angle in terms of the radius of the glass sphere containing the electrons (Materny & Mohaghegh, 2025). In doing so, the following relationship between diffraction ring radius r, bulb radius $R = 65 \cdot 10^3[m]$, the de Broglie wavelength of the electrons λ and the lattice spacing d is derived from the Bragg condition in 2.3.

$$r = \frac{2R}{d} \cdot n \cdot \lambda \quad n = 1, 2, 3, \ldots \tag{2.4}$$

The following relationship above (2.4) demonstrates a linear relationship between the diffraction ring and the de Broglie wavelength of the accelerated electron. This proportionality will be used to calculated the specific lattice spacing of the polycrystalline graphite film which coats the copper lattice. In sum, the wave-like nature of the electron shall be demonstrated through the calculation of the hexagonal lattice spacing of the polycrystalline graphite film via electron diffraction.

To analyze the latter relationship of electromagnetic waves behaving like particles, the Compton scattering effect will be explored. To observe said Compton scattering, a copper X-ray tube will be used, and its scattering behavior across a Lithium Fluoride sample will be analyzed.

To confirm the usage of a copper X-ray tube, the Bremsstrahlung radiation of the copper x-rays will be analyzed across a variety of angles after being reflected from the Lithium Fluoride sample. Bremsstrahlung radiation refers to a form of electromagnetic radiation which is emitted when a charged particle undergoes deceleration due to the deflection off of the electric field of a nucleus. In the context of this experiment, photons are emitted from a heated copper element, which are incident on a Lithium Fluoride sample. As the photons are incident to the LiF sample, they interact directly with the electric field of the free electrons inside of the nucleus. When the inner-shell electrons are ejected due to these incident photons, the emitted photons become characteristic x-rays for specific angles. These angles yield characteristic X-rays which are theoretically denoted as transitions K_α and K_β for different nuclear orders. After this Bremsstrahlung radiation is examined, Compton scattering is observed experimentally through the analysis of transmission rate dependence on wavelength. Compton scattering refers to when a photon interacts directly with a charged particle, causing it to scatter with less energy then it started with. As a result, the frequency of the resultant photon drops, and its wavelength increases. By analyzing the dependence of the wavelength of the scattered photons against the transmission rate of photons through an aluminum absorber positioned at various configurations about a plastic sample, the Compton wavelength λ_c can be determined–the difference in wavelength due to scattering and loss of energy for a scattering angle $\alpha = \frac{\pi}{2}$:

$$\lambda_c = \lambda_2 - \lambda_1 = \frac{h}{m_e c} \approx 2.426 \cdot 10^{-12}[m] \quad \text{(Materny \& Mohaghegh, 2025)} \tag{2.5}$$

Here, λ_2 and λ_1 are the wavelengths from before and after the Compton scattering of the photons, their difference yielding the Compton wavelength λ_c. Experimentally, this value is calculated by means of taking the ratio of dead-time τ normalized transmission rates $T(\theta)$, defined as written below. Using equation 2.6, the formula is inverted and a linear trend is constructed. By construction of this linear trend, transmission rates T can be semi-trivially converted into wavelengths λ for various scattering configurations. By subtracting the appropriate wavelengths, one achieves the difference in wavelengths exactly seen in equation 2.5:

$$T(\lambda) = T(\theta) = \frac{N_2^*(\theta)}{N_1^*(\theta)}, \quad N_i^* = \frac{N}{1 - \tau N} \tag{2.6}$$

In the usual case, the wavelength of the scattered x-ray photons can be calculated as the lattice spacing of the Lithium Fluoride (LiF) element is known $d_{LiF} \approx 201.4 \cdot 10^{-12}[m]$ through the formula below:

$$\lambda = 2 d_{LiF} \sin(\theta) \tag{2.7}$$

In equation 2.6, N_i^* is the normalized pulse rate of x-rays detected, where τ is the dead time of the sensor. Due to the high frequencies used (X-ray frequency range) it is crucial to normalize results with respect to the dead time of the sensor for greater accuracy. After these pulse rates are normalized, the exact transmission rates of the various setups can be calculated

by simply varying which pulse rates N_i^* are compared by means of a ratio. In doing so, the exact effects of Compton scattering can be observed, as the plastic material across which the x-rays deflect is at an orientation exactly $\frac{\pi}{2}$ radians from the incident trajectory, allowing one to calculate the Compton wavelength λ_c, the main calculated result of this sub-investigation. With this, all necessary theory has been discussed to successfully observe the desired phenomena.

3 Setup & Experimental Procedure

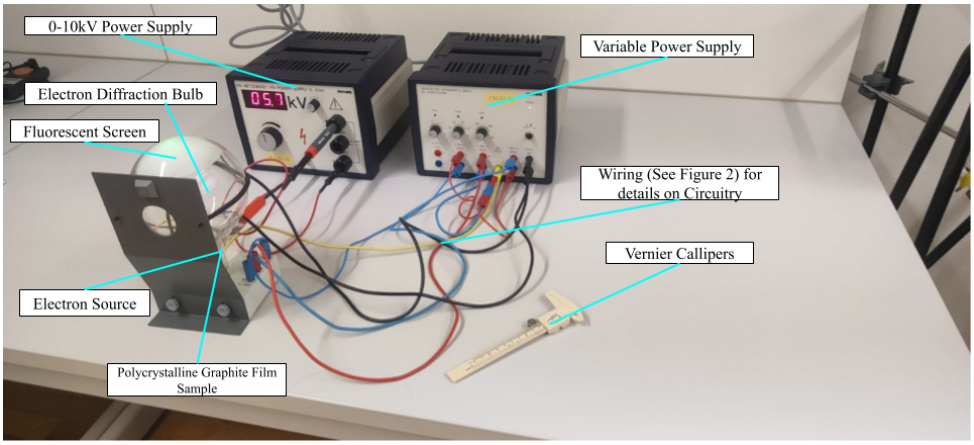

Figure 1: Annotated Setup for Electron Diffraction Investigation

To begin, the phenomena of electron diffraction was examined by considering the case of circular diffraction mediated by accelerated electrons incident on a polycrystalline graphite film coated copper lattice. As the tiled shape of the copper lattice is hexagonal, the resultant electron diffraction pattern will have 2 close rings for each fringe order, due to the varied vertical and horizontal width on the molecular level. For this aspect of the investigation, the relationship between the diffraction pattern radius of the 1st and 2nd order rings and the calculated de Broglie wavelength of the incident electrons was examined. As predicted in equation 2.4, a linear relationship between the ring radius and the de Broglie wavelength exists. From equation 2.2, it is known that the anode voltage changes the de Broglie wavelength of the electrons. Resultantly, the voltage across the acceleratory anode is varied and the ring radius measured, by applying formula 2.2 the de Broglie wavelength of the electron can be calculated, and the respective relationship examined. By extracting the slope of the relationship between ring radius and wavelength for the 1st and 2nd order diffraction patterns $n = 1, 2$, the horizontal and vertical lattice spacings of the hexagonal copper molecular structure d_1 and d_2 are determined. To prepare the electron diffraction bulb for operation, the setup had to be wired and calibrated properly to ensure efficient functionality. Below is a figure (2) of the circuit diagram as presented in the Advanced Lab II Physics Manual (Materny & Mohaghegh, 2025).

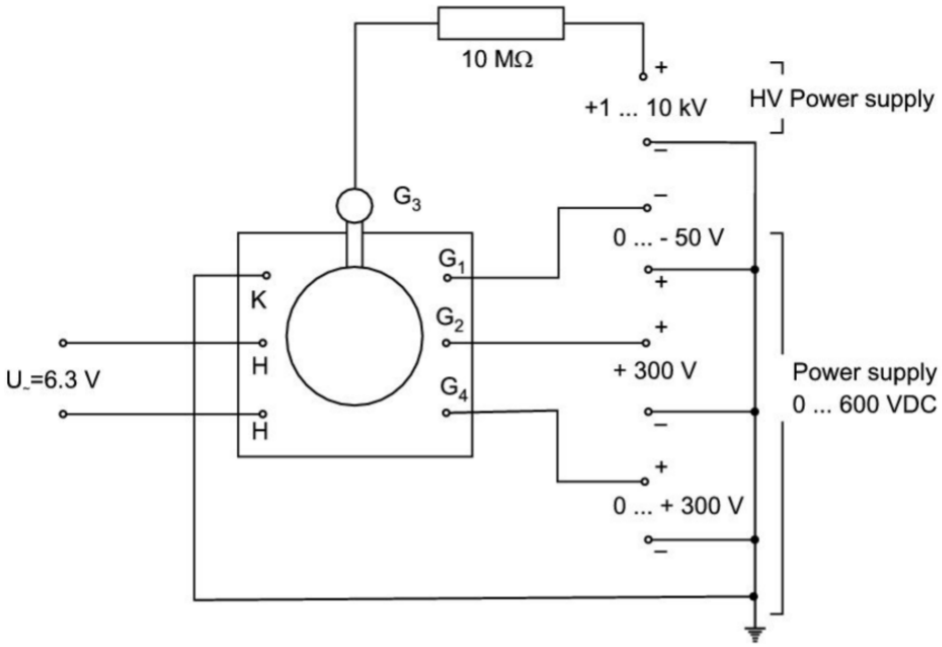

Figure 2: Circuit Diagram for Electron Diffraction Investigation (Materny & Mohaghegh, 2025)

To properly wire the setup, the acceleratory voltage across the anode is applied through terminal G_3, which runs immediately to ground. The wires which run from terminals G_1, G_2, G_4 are responsible for the fine tuning of the current across the electron source to ensure a clear visualization of the circular electron diffraction pattern. During setup, one of the most important steps of the process was ensuring that the voltages through terminals G_1, G_2, G_4 were appropriately adjusted such that a sharp diffraction pattern displayed itself on the diametrically opposed fluorescent screen. Once this pattern was nicely visible, the Vernier calipers–as seen in figure 1–were used to measure the diameter of the 1st and 2nd order fringes, and divided by 2 for the radius. This radius was then plotted against the de Broglie wavelength λ of the electrons (as calculated by formula 2.2) and the resultant lattice spacings d_1 and d_2 determined.

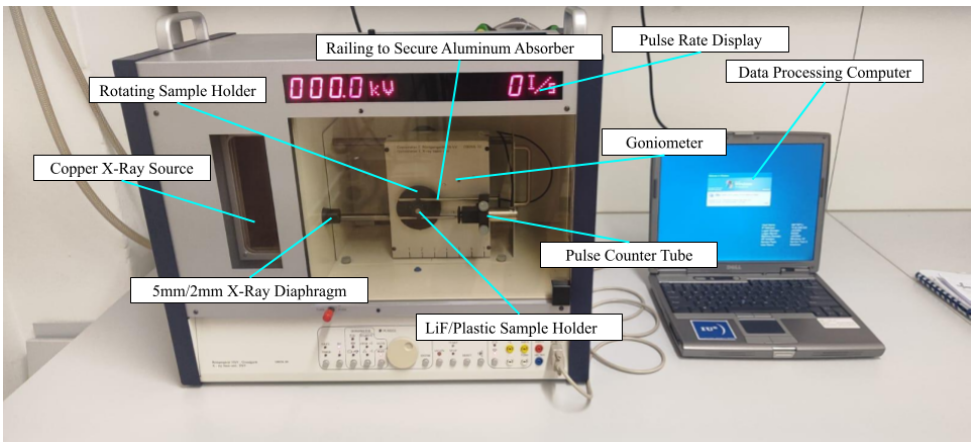

Figure 3: Annotated Setup for Compton Scattering Investigation

For the latter investigation of the particle-like scattering phenomena exhibited by X-Ray photons on a plastic sample (Compton Scattering), a machine-automated Goniometer coupled with a copper X-Ray source was utilized (See Figure 3). For the first aspect of the experiment, the Bremsstrahlung spectrum of the copper X-Ray Source was observed through the continuous rotation of a Lithium Fluoride screen placed on the rotating sample holder as annotated in figure 3. By varying the angle of the sample holder with respect to the incident X-ray beam, the specific emission spectrum of copper was analyzed via diffraction. At each angle where the Bragg condition (see equation 2.3) was fulfilled, a large peak in pulse rate would be observed, corresponding to a spectral line of copper. By analyzing the 1st and 2nd order spectra of copper, the two major transition types of the copper emission sample used were classified–as K_α and K_β transitions respectively.

After the transition Bremsstrahlung radiation spectra of copper across a Lithium Fluoride sample was examined, the transmission rate of an aluminum absorber was analyzed in order to construct the interpolated inverse relationship of the transmission rate $T(\lambda)$ and wavelength $\lambda(T)$ to be used in the calculation of the Compton wavelength λ_c. To construct this linear trend, the behavior of the pulse rate against angle θ was measured for angles from 5.5 to 11.5 degrees to the incident X-ray beam. These pulse rates N_i were then normalized to N_i^* with respect to the dead time of the count tube τ (as specified in formula 2.6), and used to calculate the transmission rates dependence on the wavelength of the scattered X-Ray photons.

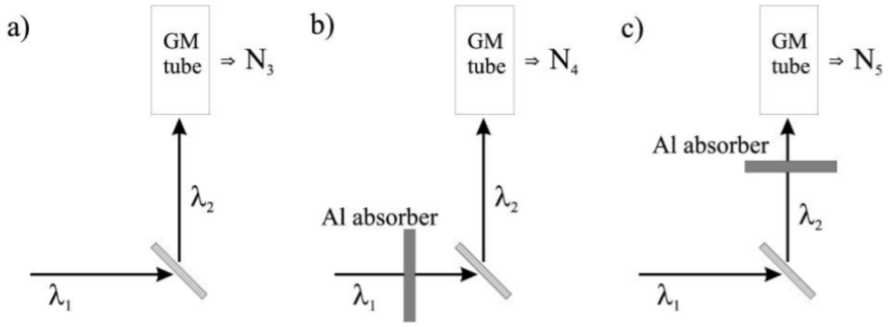

Figure 4: Schematic Procedure for Determination of Compton Wavelength λ_c, (Materny & Mohaghegh, 2025)

After the calculation of the dependence of transmission rate against wavelength for the aluminum absorber, the pulse rates for various configurations (Figure 4) of an aluminum absorber and plastic reflector (rotated to $135°$) are analyzed to determine the two transmission rates, and consequently wavelengths required to yield the Compton wavelength estimate. While positioning, the aluminum absorber was placed as close to the plastic sample as possible as to ensure optimal absorption, after configured, the system was left for 20 minutes at a time for an accurate average pulse rate, and consequently accurate calculated Compton wavelength λ_c.

4 Results and Data Analysis

To investigate the phenomena of electron diffraction, raw data was collected investigating the relationship between electron-acceleratory anode voltage and the diameter of the 1st and 2nd order rings. To achieve sufficiently accurate measurements of the radius of the bright fringes on the fluorescent screen, the average of the inside and outside of each diffraction ring was measured, and the arithmetic mean taken. After the diameter was measured, the radius was calculated through the simple halving of each measurement. These values allowed for the examination of the relationship between de Broglie wavelength λ–calculated from the anode voltage U_A using formula 2.2–and the radius of the resultant two diffraction rings (for each hexagonal lattice spacing). For a wide range of measurements, anode voltages U_A from 4kV to 7.5kV were measured in steps of 0.5kV, and the respective diffraction radius measured. Below are the tabulated results for the raw data collected during the electron diffraction investigation.

Table 1: Raw data of anode voltage U_A against 1st and 2nd order circular diffraction radius r_1, r_2

Anode Voltage ± 0.1 [kV]	Diameter $(n=1)$ $\pm 5 \cdot 10^{-4}$ [m]	Diameter of $(n=2)$ $\pm 5 \cdot 10^{-4}$ [m]	Radius $(n=1)$ $\pm 2.5 \cdot 10^{-4}$ [m]	Radius $(n=2)$ $\pm 2.5 \cdot 10^{-4}$ [m]
4.0	0.023	0.045	0.0115	0.0225
4.5	0.02	0.039	0.01	0.0195
5.0	0.0195	0.036	0.00975	0.018
5.5	0.019	0.0355	0.0095	0.01775
6.0	0.018	0.034	0.009	0.017
6.5	0.0175	0.033	0.00875	0.0165
7.0	0.017	0.032	0.0085	0.016
7.5	0.0155	0.03	0.00775	0.015

To achieve the linear relationship between diffraction pattern radius and wavelength as desired, the de Broglie wavelength of the electrons for varying Anode Voltages must be calculated. To do so, formula 2.2 is applied, and the raw data is processed such that de Broglie wavelength λ is compared against the radius. As an example calculation, the de Broglie wavelength of an electron accelerated by an anode voltage of 4kV is given by:

$$\lambda = \frac{h}{\sqrt{2m_e e U_A}}$$
$$\lambda = \frac{6.626 \cdot 10^{-34}[Js]}{\sqrt{2(9.11 \cdot 10^{-31}[kg])(1.6 \cdot 10^{-16}[C])(4 \cdot 10^{3}[V])}}$$
$$\lambda = (194 \pm 2.43) \cdot 10^{-13}\ [m]$$

where the uncertainty is calculated using the formula detailed in the error analysis section of the report. Such afore-performed analysis is carried out for both 1st and 2nd diffraction rings to achieve both lattice spacings of the polycrystalline graphite film coated copper. Below are the two processed data tables containing the necessary information to construct a full linear relationship between wavelength λ and 1st and 2nd pattern radii r_1 and r_2, each corresponding to either the vertical d_1 or horizontal d_2 hexagonal spacing of the polycrystalline graphite film coated copper lattice.

Table 2: Diffraction Radius r_1 against λ

Radius [m]	Wavelength [m]	Error [m]
0.0115	$1.94 \cdot 10^{-11}$	$2.43 \cdot 10^{-13}$
0.01	$1.83 \cdot 10^{-11}$	$2.03 \cdot 10^{-13}$
0.00975	$1.74 \cdot 10^{-11}$	$1.74 \cdot 10^{-13}$
0.0095	$1.65 \cdot 10^{-11}$	$1.50 \cdot 10^{-13}$
0.009	$1.58 \cdot 10^{-11}$	$1.32 \cdot 10^{-13}$
0.00875	$1.52 \cdot 10^{-11}$	$1.17 \cdot 10^{-13}$
0.0085	$1.47 \cdot 10^{-11}$	$1.05 \cdot 10^{-13}$
0.00775	$1.42 \cdot 10^{-11}$	$9.45 \cdot 10^{-14}$

Table 3: Diffraction Radius r_2 against λ

Radius [m]	Wavelength [m]	Error [m]
0.0225	$1.94 \cdot 10^{-11}$	$2.43 \cdot 10^{-13}$
0.0195	$1.83 \cdot 10^{-11}$	$2.03 \cdot 10^{-13}$
0.018	$1.74 \cdot 10^{-11}$	$1.74 \cdot 10^{-13}$
0.01775	$1.65 \cdot 10^{-11}$	$1.50 \cdot 10^{-13}$
0.017	$1.58 \cdot 10^{-11}$	$1.32 \cdot 10^{-13}$
0.0165	$1.52 \cdot 10^{-11}$	$1.17 \cdot 10^{-13}$
0.016	$1.47 \cdot 10^{-11}$	$1.05 \cdot 10^{-13}$
0.015	$1.42 \cdot 10^{-11}$	$9.45 \cdot 10^{-14}$

The data above numerically demonstrates that as the radius of the diffraction pattern decreases, the wavelength decreases as well. This numerical observation is indicative of a positive linear relationship between the two quantities, as predicted by equation 2.4. To ensure that this positive linear relationship is in fact present, a linear regression is performed on the data points in tables 2 and 3, and the slope of the relationship extracted to obtain the values of the lattice spacings d_1 and d_2.

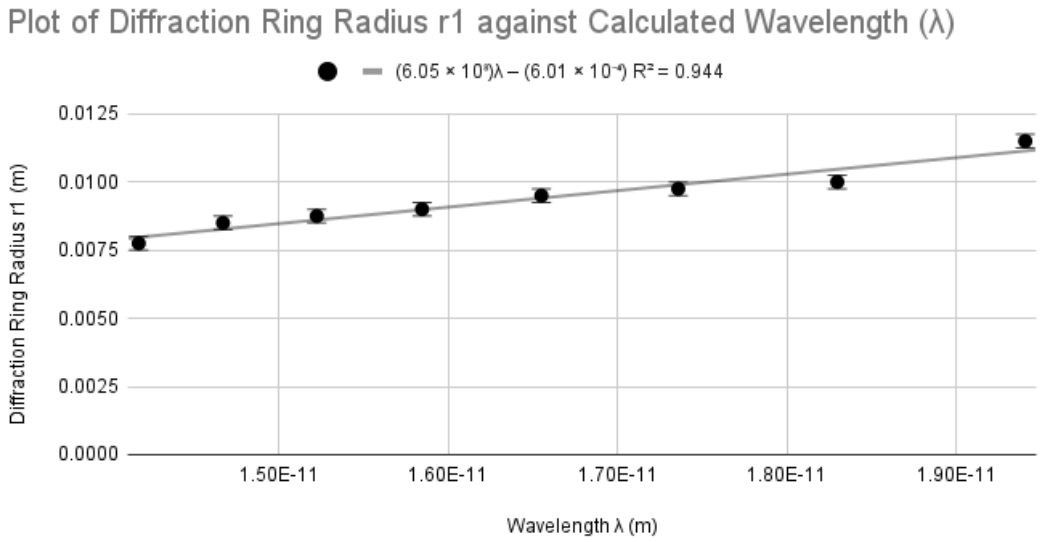

Figure 5: Plot of 1st Diffraction Ring Radius r_1 against Calculated De Broglie Wavelength λ

Indeed the plot above demonstrates a strongly correlated ($R^2 = 0.944$) positive relationship between the de Broglie wavelength λ and the diffraction ring radius. Such relationship is described by the equation:

$$r_1 = (6.05 \cdot 10^8)\lambda - (6.01 \cdot 10^{-3}) \tag{4.1}$$

where the error of the slope is given by $\pm 6.15 \cdot 10^7$. Such a relationship can be immediately regarded as physically accurate, as when the wavelength of a wave increases, its frequency in

turn decreases, leading to a drop in energy. A consequent drop in energy then directly implies a rise in diffraction ring radius as the incident waves are diffracted more strongly. Extracting the slope of equation 4.1 and employing the theory developed by equation 2.4, one can trivially calculate the vertical hexagonal lattice spacing of the graphite film coated copper lattice. Below is the complete calculation of said lattice spacing by method of substitution into equation 2.4.

$$\text{Slope} = 6.05 \cdot 10^{8} = \frac{2R}{d_1} \cdot n \tag{4.2}$$

As the literature value of the glass bulb used during the experiment is $R = 65[mm]$ and the first order fringe is examined here $n = 1$, one can rearrange equation 4.2 for the lattice spacing d_1.

$$d_1 = \frac{2R \cdot n}{6.05 \cdot 10^{8}} = \frac{2(0.065)(1)}{6.05 \cdot 10^{8}} = 2.15 \times 10^{-10} \text{ [m]} \approx 215 \text{ [pm]} \tag{4.3}$$

With error of the vertical lattice spacing calculated through root sum of square partial derivative error propagation, the final value for the slit spacing of the polycrystalline graphite film coated copper with absolute error is given by:

$$\boxed{d_1 = (21.5 \pm 2.19) \cdot 10^{-11} \text{ [m]}} \tag{4.4}$$

Comparing this value to the theoretical value for the longest lattice spacing of such a copper sample $d_1 \approx 213$ [pm], the calculated result adheres to the expected literature value to a commensurable degree.

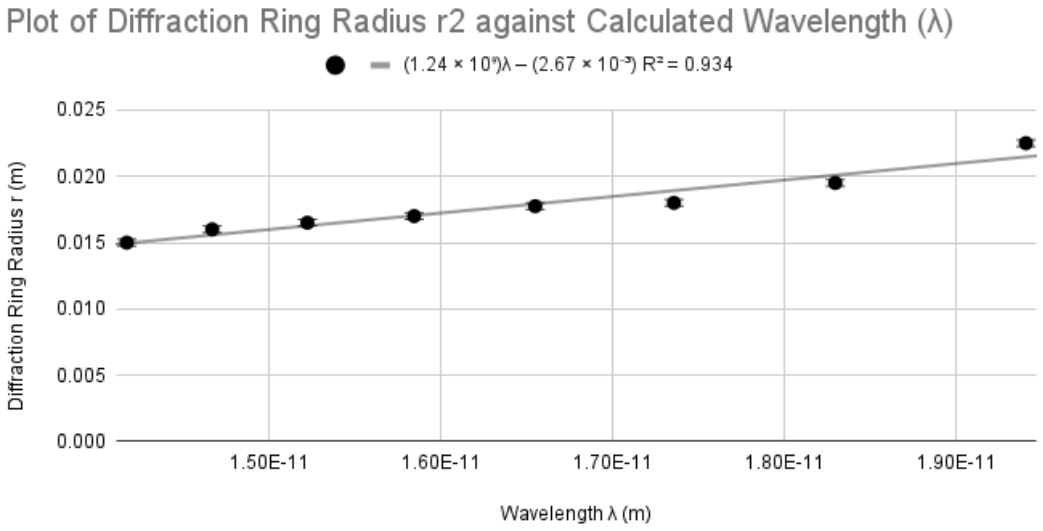

Figure 6: Plot of 2nd Diffraction Ring Radius r_2 against Calculated De Broglie Wavelength λ

In exact same fashion as to how the longer lattice spacing d_1 was calculated, the secondary lattice spacing of the polycrystalline film d_2 will be calculated through the slope of the regression result given in figure 6 above. In comparison to the regression performed for the primary lattice spacing d_1, the fit is slightly less accurate, with an R^2 value of 0.934 and a slope uncertainty of $\pm 1.37 \cdot 10^8$. This is likely due to the larger radius measurements, and therefore higher susceptibility to error due to greater fluctuation of measurement. Said aforementioned regression yields a relationship between the secondary diffraction ring radius r_2 against de Broglie wavelength λ given by:

$$r_2 = (1.24 \cdot 10^9)\lambda - (2.67 \cdot 10^{-3}) \tag{4.5}$$

Extracting the slope of this relationship as done previously, one can equate this to the proportionality constant of the radius-wavelength relationship (2.4) to calculate the secondary lattice spacing of the molecular diffraction grating, where the order is still 1, however the ring is larger due to the irregular hexagonal lattice spacing.

$$\implies d_2 = \frac{2R \cdot n}{1.24 \cdot 10^9} = \frac{2(0.065)(1)}{1.24 \cdot 10^9} = 1.05 \cdot 10^{-10} \text{ [m]} \approx 105 \text{ [pm]} \tag{4.6}$$

Again by method of root sum of square partial derivative error propagation, the absolute error of the secondary lattice spacing d_2 is calculated, yielding a final value of the lattice spacing, with error, of:

$$\boxed{d_2 = (10.5 \pm 1.15) \cdot 10^{-11} \text{ [m]}} \tag{4.7}$$

In comparison to the literature value for the secondary lattice spacing of a polycrystalline graphite film coated copper lattice, it is slightly more deviant, with a literature value of $d_2 = 123$ [pm]. This larger deviation is likely due to the more sensitive dependence of the radius on the wavelength of the particle, for its fringe lies farther from the central maximum. Alternatively, measurement errors due to the lessened intensity of the larger ring could be attributed to the offset calculated value from that of the theoretical. However, the two results are not unacceptably deviant from one another and the results obtained are still physically relevant.

The next aspect of this investigation focuses on the demonstration of electromagnetic waves (X-Ray Photons) behaving as particles through Compton Scattering. The first measurement series taken was the pulse rate against varied incident angle on a Lithium Fluoride to analyze the Bremsstrahlung radiation spectrum exhibited by the copper X-Ray source. For this measurement series, the voltage applied to the source was 35kV, and was passed through an optical diaphragm of radius 5mm. The results were tabulated and plotted in a way such that the 1st and 2nd order diffraction peaks due to satisfied Bragg Condition could be visualized as seen in figure 7.

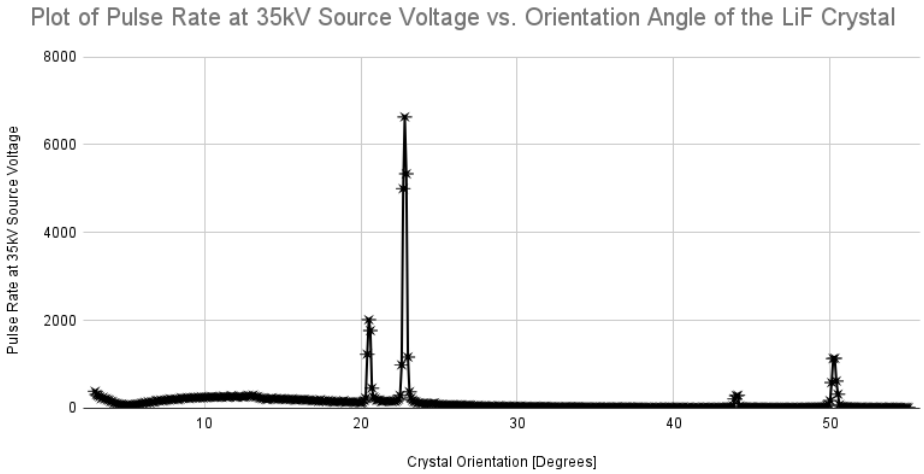

Figure 7: Plot of Pulse Rate for 35kV Source Voltage against Angle of the LiF Crystal

The plot above very nicely demonstrates the existence of a discrete nuclear spectrum of Bremsstrahlung radiation. In figure 7, two families of peaks are observed, the first corresponding to 1st order diffraction of the K_α and K_β transition states, and the second family of peaks for angles $> 40°$ corresponding to the 2nd order diffraction pattern of the Bremsstrahlung spectra. Extracting the maxima of plot 7, one can determine the corresponding wavelength of the peak by applying formula 2.3 and consequently the exact energy levels of the K_α and K_β transition states by referencing the relativistic wavelength dependent energy of a photon $E = \frac{hc}{\lambda}$. In doing so, the values obtained for the transition energy levels of the copper emitted X-Rays are given in table 4 below and compared to their theoretical values (Yvon, 2025):

Table 4: Calculated Energy Levels of Bremsstrahlung Radiation Spectra for Copper X-Rays

Angle of Peak (deg)	Theoretical Transition	Calculated Wavelength [m]	Calculated Energy [J]	Error of Energy $\pm[J]$	Theoretical Characteristic Energy of X-Ray [J]
20.5	K_β	$1.41 \cdot 10^{-10}$	$1.41 \cdot 10^{-15}$	$3.77 \cdot 10^{-16}$	$1.43 \cdot 10^{-15}$
22.8	K_α	$1.56 \cdot 10^{-10}$	$1.27 \cdot 10^{-15}$	$3.03 \cdot 10^{-16}$	$1.29 \cdot 10^{-15}$
44.1	K_β	$1.40 \cdot 10^{-10}$	$1.42 \cdot 10^{-15}$	$2.93 \cdot 10^{-16}$	$1.43 \cdot 10^{-15}$
50.3	K_α	$1.55 \cdot 10^{-10}$	$1.28 \cdot 10^{-15}$	$2.13 \cdot 10^{-16}$	$1.29 \cdot 10^{-15}$

As one can see, the calculated energy levels for the emission spectra of Copper significantly adhere to the pre-established theoretical description as provided by (Yvon, 2025). Using this information, one can state with confidence the wavelengths used during the Compton scattering experiment. Moving forward, the dead time τ normalized pulse rates N_1^*, N_2^* of X-Rays deflected from a Lithium Fluoride crystal are determined with and without the present of an intermediary aluminum absorber, and its corresponding transmission rate T calculated using formula 2.6. These measurements are performed for angles between 5.5 to 11.5 degrees in steps of 0.5. In doing so, a direct linear relationship between transmission rate T and scattered wavelength is determined to be used as interpolatory machinery during the explicit investigation of Compton scattering. Below is the plot (Figure 8) of the wavelength of the X-Rays against transmission rate $T = \frac{N_2^*(\theta)}{N_1^*(\theta)}$, a clearly linear relationship is shown.

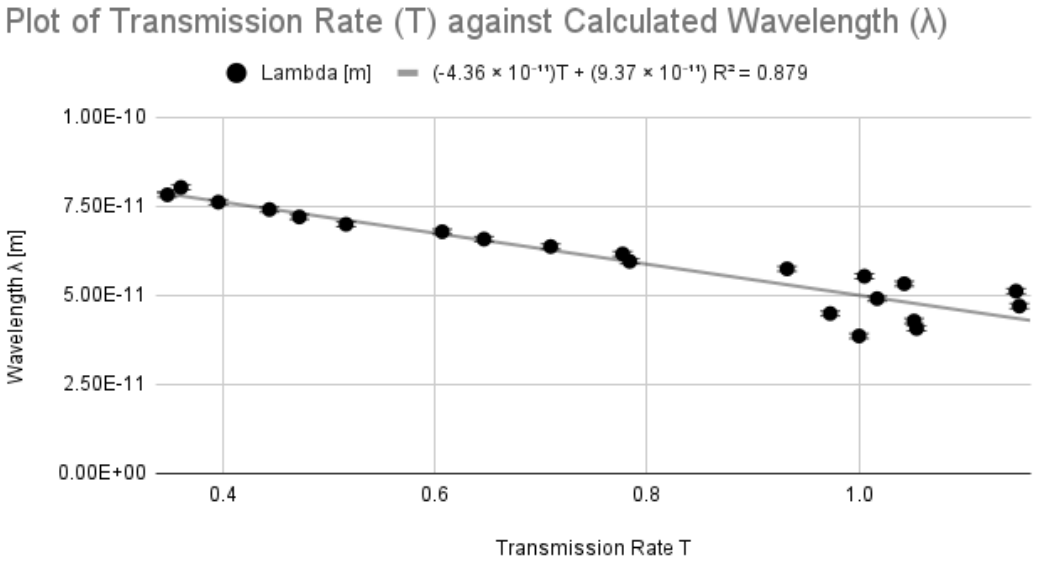

Figure 8: Enter Caption

The figure demonstrates with a correlation of $R^2 = 0.879$ and slope uncertainty of $\pm 3.71 \cdot 10^{-12}$ $[mImp^{-1}s]$ that a linear trend between the wavelength of scattered X Ray photons and transmission rate is directly correlated by the equation:

$$\lambda = (-4.36 \cdot 10^{-11})T + (9.47 + 10^{-11}) \tag{4.8}$$

This equation will be used later to directly translate between transmission rates after Compton Scattering and the wavelength of such scattered X-Ray photons. For the last aspect of this investigation, the Lithium Fluoride crystal was replaced for a plastic media rotated to $135°$ such that an exact angle of $\alpha = \frac{\pi}{2}$ is made between the incident and scattered beam of X-Ray photons, allowing for Compton scattering to efficiently occur. After this was done, the pulse rates through the count tube were measured for configurations according to figure 4 as seen in the setup section. The extracted values of the count rates N_3, N_4, N_5, and their respective normalized values N_3^*, N_4^*, N_5^* (using equation 2.6) are given in table 5 below.

Table 5: Table of Calculated Count Rates for Various Absorber Configurations

	Count Rate for 35kV [Imp/s]	Dead Time Normalized Count Rates [Imp/s]	Error of the Normalized Count Rates $\pm[Imp/s]$
N3	288.3	287.238	1.054
N4	109.7	102.334	1.020
N5	96.3	88.703	1.018

Using the values tabulated above, one can calculated the corresponding transmission rates of the aluminum absorber before and after Compton scattering against the 135° oriented plastic sample. Below is the calculation of these aforementioned transmission rates T_1 and T_2, each of which will be applied to the interpolated equation 4.8 to calculate the wavelengths before and after the Compton scattering event. Should a difference in wavelength be present, such difference is referred to as the Compton wavelength λ_c. To calculate the transmission coefficients T_1 and T_2, one substitutes the normalized values for N_3^*, N_4^* and N_5^* in to the equations below as follows:

$$T_1 = \frac{N_4^*}{N_3^*}, \qquad T_2 = \frac{N_5^*}{N_3^*} \tag{4.9}$$

$$\implies T_1 = \frac{102.334 \text{ [Imp/s]}}{287.238 \text{ [Imp/s]}}, \qquad T_2 = \frac{88.703 \text{ [Imp/s]}}{287.238 \text{ [Imp/s]}} \tag{4.10}$$

$$T_1 = 0.356 \pm 3.78 \cdot 10^{-3}, \qquad T_2 = 0.309 \pm 3.72 \cdot 10^{-3} \tag{4.11}$$

With the corresponding transmission rates before and after the Compton scattering event calculated, one can substitute these values into the obtained interpolated relationship to find estimates for the wavelengths of the X-Rays before and after the Compton scattering event λ_1 and λ_2. Substituting these values in to the equation 4.8, one achieves values for λ_1 and λ_2 of:

$$\lambda_1 = (7.82 \pm 0.133) \cdot 10^{-11} \text{ [m]} \qquad \lambda_2 = (8.02 \pm 0.116) \cdot 10^{-11}) \text{ [m]} \tag{4.12}$$

As the Compton wavelength is defined as the difference of these two wavelengths, one achieves a final value with uncertainty of the Compton wavelength λ_c of:

$$\boxed{\lambda_c = \lambda_2 - \lambda_1 = (2.07 \pm 1.76) \cdot 10^{-12} [m]} \tag{4.13}$$

In comparison to the theoretical value for the Compton wavelength $\lambda_c \approx 2.426 \cdot 10^{-12}$ [m] (Materny & Mohaghegh, 2025), the calculated result adheres to the theoretical value to a commensurable degree.

5 Error Analysis

For all errors involving the slope of the graph, the uncertainty of the slope was approximated using the built-in function (LINEST), which works by approximating the linear slope of a set of data points through the least squares method. As a byproduct, the error of the slope is given in absolute form. Due to the efficiency of this method, and the large quantity of graphs, it was the clear choice for this investigation. For all errors involving numerical calculations with propagated error, the root sum of squares method (RSS) was employed. This method involves

calculating the propagated error of a formulaic value by computing all partial derivatives with respect to all error-prone parameters, and taking it under a square root. The formula for this is given below.

$$\Delta y = \sqrt{\sum_{i=0}^{n} \left(\frac{\partial y}{\partial x_i} \cdot \Delta x_i \right)^2} = \sqrt{\left(\frac{\partial y}{\partial x_1} \cdot \Delta x_1 \right)^2 + \cdots + \left(\frac{\partial y}{\partial x_n} \cdot \Delta x_n \right)^2} \tag{5.1}$$

The error of the value of the de Broglie wavelength relies on precise voltage measurements. The instrumental error of the anode voltage was ± 0.1kV, which propagated into the wavelength calculation. Additionally, fluctuations in power supply could introduce errors in the electron acceleration process. The error of the wavelength was calculated using the following formula:

$$\Delta\lambda = \left| -\frac{h}{2} \frac{2m_e e}{(2m_e e U_A)^{3/2}} \right| \Delta U \tag{5.2}$$

The diameter of the diffraction ring was measured using a vernier calliper with an instrumental uncertainty of $\pm 5 \cdot 10^{-4}$m. Accordingly, the error of the radius would be $\pm 2.5 \cdot 10^{-4}$m. Errors in the radius measurement affect the calculated lattice spacing. From the plots of the diffraction ring radii (r1 and r2) against the calculated wavelength, the slopes of the linear fit and their error using the LINEST function were obtained to be $6.15 \cdot 10^7$ and $1.37 \cdot 10^8$ accordingly. They propagate into the lattice spacing calculation according to the following formula:

$$\Delta d = | -\frac{2R \cdot n}{m^2} | \Delta m \tag{5.3}$$

$$\Delta d_1 = \left| -\frac{2 \cdot 0.065 \cdot 1}{(6.05 \cdot 10^8)^2} \right| 6.15 \cdot 10^7 = 2.19 \cdot 10^{-11} [m] \tag{5.4}$$

$$\Delta d_2 = \left| -\frac{2 \cdot 0.065 \cdot 1}{(1.24 \cdot 10^9)^2} \right| 1.37 \cdot 10^8 = 1.15 \cdot 10^{-11} [m] \tag{5.5}$$

where m is the slope of the linear fit, $R = 65$mm is the given radius of the bulb with no uncertainty and for two innermost interference rings n=1. The final uncertainties for the lattice spacing values were obtained to be $2.19 \cdot 10^{11}$ [m] and $1.15 \cdot 10^{11}$ [m]. The determination of X-ray wavelength characteristics depended on precise angle measurements, which had an instrumental uncertainty of ± 0.1[Deg]. The angles for the four peaks were obtained from the pulse rate against the crystal orientation graph, where pulse rate measurements had an instrumental error of ± 1 [Imp/s]. For the four peaks on the graph, wavelength and energy were calculated. The error of wavelength λ was calculated using the following formula propagated from equation 2.3:

$$\Delta\lambda = \frac{2d\cos(\theta)}{n} \Delta\theta = \frac{2 \cdot 201.4 \cdot 10^{-12} \cos(\theta)}{n} \Delta\theta \tag{5.6}$$

where d is the lattice constant with 0 uncertainty, n=1 for the first two peaks and n=2 for the next

two peaks. The error of the corresponding energy was calculated using the following formula:

$$\Delta E = \left|\frac{c \cdot h}{\lambda^2}\right| \Delta\lambda = \frac{299792458 \cdot 6.62607015 \cdot 10^{-34}}{\lambda^2}\Delta\lambda \tag{5.7}$$

For the determination of the transmission rate for aluminium experiment,the pulse rate, again had an instrumental error of 1 Imp/s, errors for the normalized values were obtained using the formula:

$$\Delta N^* = \frac{\Delta N}{(1-\tau N)^2} \tag{5.8}$$

where $\tau = 90\mu s$ is the dead time correction factor. Error for the transmission rate values was calculated using the following formulas:

$$\Delta T_1 = \sqrt{\frac{\Delta N_4^{*2}}{N_3^{*2}} + \left(\frac{N_4^*}{N_3^{*2}}\right)^2 \Delta N_3^{*2}} \tag{5.9}$$

$$\Delta T_1 = \sqrt{\frac{1.02^2}{287.24^2} + \left(\frac{102.33}{287.24^2}\right)^2 1.054^2} = 0.0038 \tag{5.10}$$

$$\Delta T_2 = \sqrt{\frac{\Delta N_5^{*2}}{N_3^{*2}} + \left(\frac{N_5^*}{N_3^{*2}}\right)^2 \Delta N_3^{*2}} \tag{5.11}$$

$$\Delta T_2 = \sqrt{\frac{1.02^2}{287.24^2} + \left(\frac{88.70}{287.24^2}\right)^2 1.054^2} = 0.0037 \tag{5.12}$$

and the errors of the wavelength values were calculated using equation 5.6. The calculated wavelength as a function of transmission rate was plotted and the error of the linear fit was obtained using the LINEST function. $\pm\Delta m_{transmission} = 3.71 \cdot 10^{-12}$. The linear regression equation was used to calculate the λ_1 and λ_2 wavelength. Accordingly, the errors of the λ_1 and λ_2 were calculated using the formula:

$$\Delta\lambda = \sqrt{(T \cdot \Delta m_{transmission})^2 + (m_{transmission} \cdot \Delta T)^2} \tag{5.13}$$

The obtained values were to be: $\Delta\lambda_1 = \pm 1.33 \cdot 10^{-12}[m]$ and $\Delta\lambda_2 = \pm 1.16 \cdot 10^{-12}[m]$

$$\Delta\lambda_c = \sqrt{(\Delta\lambda_1)^2 + (\Delta\lambda_2)^2} \tag{5.14}$$

The final error for the Compton wavelength obtained to be $\Delta\lambda = \pm 1.76 \cdot 10^{-12}[m]$ Despite the presence of experimental uncertainties, the obtained results demonstrate a strong agreement with theoretical predictions. The primary limitation in precision was linked to the visual measurements of diffraction rings and count rate fluctuations in the Compton experiment.

6 Discussion

Looking back on the results of the experiment, it is clear that this investigation strongly supports the fundamental principles of wave-particle duality. In the electron diffraction experiment, the relationship between de Broglie wavelength and diffraction ring radius was successfully investigated. The plots of diffraction ring radius against wavelength performed linear correlation, and confirmed the linear dependence as stated in the equation 2.4. This reflects the wave-like behaviour of electrons. The determined values for the lattice spacings of the polycrystalline graphite-coated copper film were: $d_1 = (21.5 \pm 2.19) \cdot 10^{-11}$m and $d_2 = (10.5 \pm 1.15) \cdot 10^{-11}$m. These values closely agree with the literature values, especially d_1 falls within the expected range of 213 pm. The larger deviation for d_2 from the theoretical value can be explained by the measurement uncertainties in determining the outer diffraction ring radius as the outer ring was thicker and more blurred. Overall some systematic deviations in this experiment were expected given the challenging visual measurement methods and non-precise anode voltage settings.

The Compton scattering experiment further demonstrated the particle-like nature of waves. The analysis of the Bremsstrahlung spectrum of a copper X-ray source and measurement X-ray transmission through an aluminium absorber, identified the characteristic X-ray transitions of copper. The calculated energy levels of K_α and K_β obtained to be:

$$E_{K_\alpha} = (1.27 \pm 0.30) \times 10^{-15} \text{ [J]} \tag{6.1}$$

$$E_{K_\beta} = (1.41 \pm 0.38) \times 10^{-15} \text{ [J]} \tag{6.2}$$

After that, transmission rates before and after Compton scattering were calculated as:$T_1 = 0.356 \pm 3.78 \cdot 10^{-3}$ and $T_2 = 0.309 \pm 3.72 \cdot 10^{-3}$. The transmission values were used to interpolate corresponding wavelengths before and after scattering. The obtained values were: $\lambda_1 = (7.82 \pm 0.133) \times 10^{-11}$ m and $\lambda_2 = (8.02 \pm 0.116) \times 10^{-11}$m. The difference in the values represents the experimentally obtained Compton wavelength shift:

$$\lambda_c = (2.07 \pm 1.76) \cdot 10^{-12}[m]. \tag{6.3}$$

This value is in agreement with the theoretical Compton wavelength when the scattering angle is $\pi/2$, the theoretical value for λ_c is $\lambda_c = 2.426 \cdot 10^{-12}$ m. The observed deviation can be caused by systematic uncertainties in the transmission rate measurements and the detector's response time. Even though the dead-time correction was applied to all measured values, small fluctuations in the count rate can still occur. Overall this experiment successfully validated the two-nature behavior of electromagnetic waves. The agreement between experimental and theoretical values confirms the accuracy of the experimental methods. Future improvements could include: the use of higher-resolution imaging techniques for diffraction ring measurements and better detector sensitivity for X-ray transmission analysis.

7 Conclusion

In this investigation, the fundamental principles of wave-particle duality were successfully examined through the experimental analysis of electron diffraction and Compton scattering. The experiments conducted provided substantial evidence for the dual nature of matter and electromagnetic waves, as predicted by quantum mechanics. For the electron diffraction experiment, the relationship between the de Broglie wavelength and the diffraction ring radius was studied in detail. By varying the anode voltage of the electron beam and measuring the resulting diffraction pattern, the hexagonal lattice spacings of the polycrystalline graphite-coated copper film were determined. The calculated values of the lattice spacings were found to be:

$$d_1 = (21.5 \pm 2.19) \times 10^{-11} \text{ m} \tag{7.1}$$

$$d_2 = (10.5 \pm 1.15) \times 10^{-11} \text{ m} \tag{7.2}$$

These values demonstrate a strong agreement with theoretical expectations, particularly for the primary lattice spacing, which closely aligns with the literature value of 213 pm. The slightly larger deviation in the secondary lattice spacing is likely attributed to measurement uncertainties and the increased difficulty in precisely determining the outer diffraction ring radius. Nonetheless, the positive linear relationship between the diffraction ring radius and de Broglie wavelength λ, as predicted by equation 2.4, was successfully observed. For the Compton scattering experiment, the Bremsstrahlung radiation spectrum of a copper X-ray source was analyzed through diffraction from a Lithium Fluoride (LiF) crystal. By measuring the pulse rate at varying incident angles, the characteristic X-ray transitions of copper were identified. The calculated energy levels for the K_α and K_β energy transitions were found to be:

$$E_{K_\beta} = (1.41 \pm 0.38) \times 10^{-15} \text{ [J]} \tag{7.3}$$

$$E_{K_\alpha} = (1.27 \pm 0.30) \times 10^{-15} \text{ [J]} \tag{7.4}$$

These values closely match the theoretical expectations, confirming the accuracy of the measurements. The final step in the Compton scattering experiment involved determining the Compton wavelength shift by analyzing the dependence of X-ray transmission rates on scattered photon wavelengths. The unit-less transmission rates before and after Compton scattering were found to be:

$$T_1 = 0.356 \pm 3.78 \times 10^{-3} \tag{7.5}$$

$$T_2 = 0.309 \pm 3.72 \times 10^{-3} \tag{7.6}$$

By applying the experimentally derived linear relationship between wavelength λ and transmission rate T, the wavelengths of X-Ray photons before and after Compton scattering were calculated to be:

$$\lambda_1 = (7.82 \pm 0.133) \times 10^{-11} \text{ m} \tag{7.7}$$

$$\lambda_2 = (8.02 \pm 0.116) \times 10^{-11} \text{ m} \tag{7.8}$$

From these values, the experimentally determined Compton wavelength shift was similarly obtained through the evaluation of their difference:

$$\lambda_c = (2.07 \pm 1.76) \times 10^{-12} \text{ m} \tag{7.9}$$

This result aligns well with the theoretical Compton wavelength for a scattering angle of $\frac{\pi}{2}$, which is given as $\lambda_c = 2.426 \times 10^{-12}$ m. The slight deviation can be attributed to systematic uncertainties in transmission rate measurements and detector response time although normalized results were calculated. Despite such minor deviations due to these measurement uncertainties, the overall results of this investigation strongly support the theoretical prediction of wave particle duality. The observed agreement between experimental and theoretical values for the electron diffraction and Compton scattering experiment demonstrates direct evidence for the dual nature of both matter and electromagnetic waves.

References

Materny, P. D. A., & Mohaghegh, D. F. (2025). Advanced physics lab ii manual. *Constructor University*.

Yvon, J. (2025). Table of x-ray emission lines. *Horiba, World Leader in Micro-Analysis*.